

Loss Design for Single-carrier Joint Communication and Neural Network-based Sensing

Charlotte Muth, Benedikt Geiger, Daniel Gil Gaviria and Laurent Schmalen
Communications Engineering Lab (CEL), Karlsruhe Institute of Technology (KIT)
Hertzstr. 16, 76187 Karlsruhe, Germany, Email: {first.last}@kit.edu

Abstract—We evaluate the influence of multi-snapshot sensing and varying signal-to-noise ratio (SNR) on the overall performance of neural network (NN)-based joint communication and sensing (JCAS) systems. To enhance the training behavior, we decouple the loss functions from the respective SNR values and the number of sensing snapshots, using bounds of the sensing performance. Pre-processing is done through conventional sensing signal processing steps on the inputs to the sensing NN. The proposed method outperforms classical algorithms, such as a Neyman-Pearson-based power detector for object detection and ESPRIT for angle of arrival (AoA) estimation for quadrature amplitude modulation (QAM) at low SNRs.

Index Terms—Joint communication and sensing, Neural networks, Angle estimation, Object detection, 6G

I. INTRODUCTION

Communication as well as sensing are vital services for our hyper-connected society. Sustainable and efficient solutions are extremely relevant in modern applications. An increase in spectral and energy efficiency is achieved by combining radio communication and sensing into one joint system instead of operating two separate systems. Therefore, this work focuses on the co-design of both functionalities in a single joint communication and sensing (JCAS) system. The future 6G network is expected to natively support JCAS by extending the object detection to objects without communication capabilities, and performing general sensing of the surroundings [1]. With this approach, we expect to increase spectral efficiency by making spectral resources accessible for sensing while maintaining their use for communication, as well as an increase in energy efficiency because of the dual use of a joint waveform.

There is growing interest in data-driven approaches based on machine learning (ML) since they can overcome deficits, such as hardware impairments, faced by algorithms based on model-based techniques [2], [3]. Algorithms including ML are expected to be prevalent in 6G, as its use has matured in communication and radar processing [1]. ML approaches have been studied separately for communication systems [4], [5], and in the context of radar [6], [7]. In [2], [8], an autoencoder (AE) for JCAS in a single-carrier system has been proposed, performing close to a maximum a posteriori ratio test detector benchmark for single snapshot sensing of one radar target. The work of [3] extends these methods

This work has received funding from the German Federal Ministry of Education and Research (BMBF) within the projects Open6GHub (grant agreement 16KISK010) and KOMSENS-6G (grant agreement 16KISK123).

to an orthogonal frequency-division multiplexing (OFDM) waveform, which is a well-known technique to combine communication and radar [9], [10]. They demonstrate the potential of deep-learning-based sensing to mitigate hardware mismatches. However, their research is limited to single snapshot estimation. Performing sensing on multiple snapshots should yield additional processing gains when targets do not move too fast.

In this paper, we study the monostatic sensing capabilities of a single-carrier wireless communication system with multiple snapshots. To reduce complexity, we investigate a single carrier transmission instead of multicarrier waveforms such as OFDM. We analyze in detail impacts on communication and sensing in different signal-to-noise ratio (SNR) environments and multi-snapshot sensing. Taking into account the different implications of missed and false detection of objects, a detector with a constant false alarm rate is designed using neural networks (NNs). We show that the deep neural network (DNN)-based sensing can outperform classical benchmark algorithms, namely a Neyman-Pearson-based power detector and ESPRIT for the angle of arrival (AoA) estimation.

Notation: \mathbb{R} and \mathbb{C} denote the set of real and complex numbers, respectively. Sets are denoted by calligraphic letters, e.g., \mathcal{X} , with the cardinality of a set being $|\mathcal{X}|$. We denote vectors and matrices with boldface lowercase and uppercase letters, e.g. vector \mathbf{x} and matrix \mathbf{X} . The element in the n -th row and k -th column of the matrix \mathbf{X} is denoted as x_{nk} . The transpose and conjugate transpose of a matrix \mathbf{X} are given by \mathbf{X}^\top and \mathbf{X}^H respectively, while the Hadamard product and the outer product are indicated with the operators \odot and \otimes . The diagonal matrix \mathbf{D} with diagonal entries \mathbf{d} is denoted as $\text{diag}(\mathbf{d})$ and the all-one vector of length N is denoted as $\mathbf{1}_N$. A circular-symmetric complex normal distribution with mean μ and variance σ^2 is denoted as $\mathcal{CN}(\mu, \sigma^2)$. Random variables are denoted as sans-serif letters, e.g., x , multivariate random variables with boldface sans-serif letters (e.g., \mathbf{x}). Mutual information and cross-entropy are denoted by $I(x_1, x_2)$ and $H(x_1 || x_2)$, respectively.

II. SYSTEM MODEL

In this paper, we consider a monostatic JCAS system, where the transmitter and the sensing receiver are co-located, i.e., part of the same base station, and are equipped with multiple antennas. Our objective is to detect a target and estimate the AoA of the reflected signal in an area of interest.

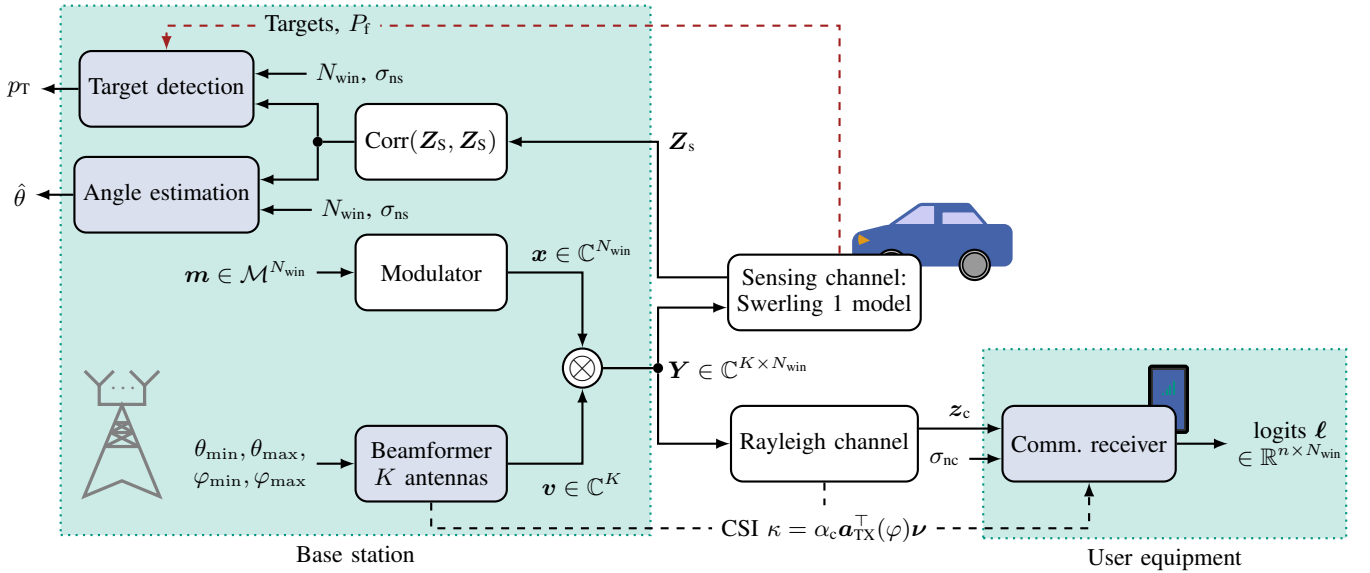


Fig. 1. JCAS system, light blue blocks are trainable NNs, red dashed paths are only active while propagating the training data

The transmit signal is simultaneously used to communicate with a user equipment (UE) equipped with a single antenna in a *different* area of interest. The communication receiver is located randomly at an azimuth angle $\varphi \in [\varphi_{\min}, \varphi_{\max}]$ following an uniform probability distribution, and the AoA of the radar target θ is drawn uniformly from $[\theta_{\min}, \theta_{\max}]$. We consider multi-snapshot sensing with N_{win} samples to provide more detailed information on multiple snapshot sensing. The system block diagram is shown in Fig. 1. The blocks shaded in blue are realized as trainable NNs.

A. Transmitter

A modulator with M different modulation symbols, while $M = 2^n$, $n \in \mathbb{N}$, transforms the data symbols $m \in \mathcal{I} := \{1, 2, \dots, M\}$ into complex symbols $x \in \mathcal{M} \subset \mathbb{C}$. We generate a vector $\mathbf{x} \in \mathbb{C}^{N_{\text{win}}}$ of N_{win} random symbols for block-wise processing. A fixed bit mapping maps a binary vector $\mathbf{b} = (b_1, \dots, b_n)^\top \in \{0, 1\}^n$ to m .

The second part of the transmitter generates digital precoding that causes beam directivity. For all K transmit antennas, a unique complex factor $v_k = g_k \exp(j\gamma_k)$ is generated for antenna $k \in \{1, 2, \dots, K\}$ with amplitude g_k and phase shift γ_k to steer the signal to our areas of interest. The beamformer inputs are the azimuth angle regions in which communication and sensing should take place, i.e. $\{\varphi_{\min}, \varphi_{\max}, \theta_{\min}, \theta_{\max}\}$. For block-wise processing, we consider a beamforming vector $\mathbf{v} \in \mathbb{C}^K$. The modulator and beamformer employ power normalization to meet power constraints.

The transmit signal $\mathbf{Y} \in \mathbb{C}^{K \times N_{\text{win}}}$ is obtained by multiplying the complex modulation symbols \mathbf{x} and the beamformer output \mathbf{v} , leading to

$$\mathbf{Y} = \mathbf{v}\mathbf{x}^\top. \quad (1)$$

B. Channels

A part of the transmit signal reaches the communication receiver while another part is reflected by the object of interest and reaches the sensing receiver co-located with the transmitter.

For communications, the signal \mathbf{Y} experiences a single-tap Rayleigh channel before being received by the communication receiver with a single antenna as

$$\mathbf{z}_c = \mathbf{1}_K^\top (\mathbf{A}_{\text{TX}}(\varphi) \odot \mathbf{Y}) \text{diag}(\boldsymbol{\alpha}_c) + \mathbf{n}_c, \quad (2)$$

with complex normal distributed $\alpha_{c,n} \sim \mathcal{CN}(0, \sigma_c^2)$ and $n_{c,n} \sim \mathcal{CN}(0, \sigma_n^2)$. The signal propagation from K antennas towards an azimuth angle φ is modeled with the spatial angle matrix $\mathbf{A}_{\text{TX}}(\varphi) = (\mathbf{a}_{\text{TX}}(\varphi_1) \dots \mathbf{a}_{\text{TX}}(\varphi_{N_{\text{win}}})) \in \mathbb{C}^{K \times N_{\text{win}}}$ whose entries are given by

$$\mathbf{a}_{\text{TX}}(\varphi) = (\exp(j\pi \sin \varphi), \dots, \exp(j\pi K \sin \varphi))^\top, \quad (3)$$

assuming the antenna spacing to exactly match $\lambda/2$ of the transmission wavelength λ . The movement of the communication receiver leads to different φ_n during an observation window. We define $\text{SNR}_c = \frac{\sigma_c^2}{\sigma_n^2}$. The total SNR needs to be corrected with the beamforming gain β_c to $\text{SNR} = \beta_c \cdot \text{SNR}_c$.

We express the sensing signal that is reflected from $T \in \{0, 1\}$ radar targets in the monostatic setup as

$$\mathbf{Z}_s = T \mathbf{a}_{\text{RX}}(\theta) \mathbf{a}_{\text{TX}}(\theta)^\top \mathbf{Y} \text{diag}(\boldsymbol{\alpha}_s) + \mathbf{N}_s, \quad (4)$$

with the radar target following a Swerling-1 model with $\alpha_{s,n} \sim \mathcal{CN}(0, \sigma_s^2)$ and $n_{s,nk} \sim \mathcal{CN}(0, \sigma_n^2)$. The spatial angle vectors relate as $\mathbf{a}_{\text{RX}}(\theta) = \mathbf{a}_{\text{TX}}(\theta)$, with θ being the AoA of the target throughout the observation window N_{win} . With a Swerling-1 model, we model scan-to-scan deviations of the radar cross section (RCS) that manifest as a change in $\alpha_{s,n}$ during N_{win} . The radial velocity of the target is assumed to be zero, so no Doppler shift occurs.

C. Sensing Receiver

At the sensing receiver, we want to detect a potential target and estimate its AoA using a linear array of K antennas in the base station. We consider multiple snapshot sensing with N_{win} snapshots, enabled by forming the auto-correlation of all considered samples across the receive antennas

$$\text{Corr}(\mathbf{Z}_s, \mathbf{Z}_s) := \frac{1}{N_{\text{win}}} \mathbf{Z}_s \mathbf{Z}_s^H \in \mathbb{C}^{K \times K}. \quad (5)$$

This signal is input to both the target detection and angle estimation blocks. The output of target detection is a probability value $p_T \in [0, 1]$ that denotes the certainty that a target is present. The angle estimation block outputs $\hat{\theta} \in [-\frac{\pi}{2}, \frac{\pi}{2}]$, which indicates the estimated azimuth AoA of the target.

D. Communication Receiver

At the communication receiver, our goal is to recover information from the received signal. We assume that the channel estimation has already been performed at the communication receiver and the precoding matrix \mathbf{v} is known; therefore, channel state information (CSI) $\boldsymbol{\kappa} = (\mathbf{A}_{\text{TX}}^T(\boldsymbol{\varphi})\mathbf{v}) \text{diag}(\boldsymbol{\alpha}_c)$ is available at the communication receiver. It is important to note that this CSI has no effect on the sensing functionality of the system. The receiver outputs are estimates of bitwise log-likelihood ratios (LLRs) $\mathbf{L} \in \mathbb{R}^{n \times N_{\text{win}}}$ that can be used as input to a soft decision channel decoder.

E. Performance Indicators

We formulate bounds on the communication throughput and the AoA estimation accuracy as performance indicators for the system.

1) *Cramér-Rao Bound*: For the estimation of the angle of a single target, the Cramér-Rao bound (CRB) is given by

$$C_{\text{CR}}(\theta) = \frac{1}{\pi^2 \cos(\theta)^2} \frac{\sigma_{\text{ns}}^2}{2N_{\text{win}}} \left[\frac{\sigma_{\text{ns}}^2 + K\beta\sigma_s^2}{K\beta^2\sigma_s^3} \right] \cdot \frac{6}{0.5K^3 - 0.5K}, \quad (6)$$

where N_{win} is the number of samples collected, θ the angle to be estimated, β the beam-forming gain, and K the number of antennas [11, Ch. 8.4]. The given CRB is a lower bound for the variance of an unbiased estimator.

2) *Bit-wise Mutual Information*: The goal of the communication receiver is to maximize the bit-wise mutual information (BMI). Maximizing the BMI is equivalent to minimizing the binary cross entropy (BCE) between true bit labels b_i and the estimated bit labels \hat{b}_i [5]. We can define it as:

$$\text{BMI}(\mathbf{b}, \hat{\mathbf{b}}) = \sum_{i=1}^{\log_2 M} I(b_i; \hat{b}_i). \quad (7)$$

The BMI is an achievable rate using binary coding and pragmatic coded modulation.

TABLE I
SIZES OF NEURAL NETWORKS

component	input layer	hidden layers	output
beamformer	4	$\{K, K, 2K\}$	$2K$
decoder	3	$\{10M, 10M, 10M, 10M\}$	$\log_2(M)$
angle estimation	$2K^2 + 2$	$\{8K, 4K, 4K, K\}$	1
detection	$2K^2 + 2$	$\{2K, 2K, K\}$	1

III. NEURAL NETWORK TRAINING AND VALIDATION

A. Neural Network Configuration

Our system is configured similarly to that of [8] with adaptations described below and NN layer dimensions given in Tab. I. The NNs consist of fully connected layers with ELU activation function in the hidden layers. We implement modulation as a classical quadrature amplitude modulation (QAM). The inputs of the beamformer are the areas of interest for sensing with $\{\theta_{\text{min}}, \theta_{\text{max}}\}$ and for communication with $\{\varphi_{\text{min}}, \varphi_{\text{max}}\}$. The output is subject to power normalization. At the communication receiver, minimum mean squared error (MMSE) equalization is performed, compensating for the random complex channel tap, to achieve better convergence along different SNR values. The outputs of the communication receiver are interpreted as LLRs for each bit. For the bit error rate (BER) calculation, we use the hard decision of these LLR values.

As stated in Sec. II, we strive to improve the performance for multiple snapshot estimation by calculating the auto-correlation matrix (ACM) $\text{Corr}(\mathbf{Z}_s, \mathbf{Z}_s)$ of the different input matrices, similarly to the first processing step of the ESPRIT algorithm. We adapt the input layer of the sensing receiver to the new input dimension. The number of input neurons of the sensing receiver is $K^2 + 2$. Two input neurons have N_{win} and σ_{ns} as inputs and allow the investigation of sensing for varying channel parameters. Specifically, our systems are trained for generalized N_{win} and σ_{ns} , allowing flexible investigation within the range of training parameters. This parameterization leads to roughly the same communication and sensing performance as systems trained individually for different N_{win} and σ_{ns} , while allowing flexible operation without requiring a change of NN weights and at the same time lowering the necessary computational complexity for training.

During training, the actual number of targets is fed to the sensing receiver in order to calculate the detection threshold that is needed to keep the false alarm rate P_f constant. This threshold is added to the output of the detection NN before applying the output sigmoid function. The output function of the angle estimation NN is $\frac{\pi}{2} \tanh(\cdot)$, normalizing the output to $\pm \frac{\pi}{2}$.

B. Loss Functions

There are 3 main components of the loss function, resulting in a multi-objective optimization, which evaluates the performance of communication, detection, and angle estimation.

We introduce a weight $w_s \in [0, 1]$, controlling the impact or perceived importance of the sensing tasks, resulting in the loss term

$$L = (1 - w_s)L_{\text{comm}} + w_s L_{\text{detect}} + w_s L_{\text{angle}}. \quad (8)$$

JCAS systems have been trained in [8] using the loss given by

$$L = (1 - w_s) \underbrace{H(\mathbf{b}||\hat{\mathbf{b}})}_{L_{\text{comm}}} + w_s \underbrace{H(\mathbf{t}||\hat{\mathbf{t}})}_{L_{\text{detect}}} + \frac{w_s}{N} \sum_{i=1}^N (\theta_i - \hat{\theta}_i)^2, \quad (9)$$

with $H(\mathbf{b}||\hat{\mathbf{b}})$ and $H(\mathbf{t}||\hat{\mathbf{t}})$ denoting the BCE between transmitter and receiver for communication and target detection respectively. While training multiple functionalities and multiple operating scenarios simultaneously, we observed a reduced performance when using a loss according to [8]. Especially the AoA estimation showed unreliable convergence, since the achievable precision, which is bounded by (6), depends significantly on the chosen N_{win} and σ_{ns} . Therefore, the impact of trainable weights can be highly perturbed by these parameters. We introduce bound-informed adaptations to ensure good behavior over a range of SNRs and observation window lengths N_{win} .

In particular, we use the formulation of the CRB in (6) for an informed modification of the loss function used for the training of NNs. Under the assumption of $\sigma_{\text{ns}}^2 \ll K\beta\sigma_s^2$, the factor $\sigma_{\text{ns}}^2/N_{\text{win}}$ describes the impact of the observation window and SNR on the bound. We modify the loss term with the correction factor $N_{\text{win}}/\sigma_{\text{ns}}^2$, achieving loss terms with similar magnitude for varying N_{win} and σ_{ns} . The proposed loss term is then given by:

$$L_{\text{angle}} = \frac{1}{N} \sum_{i=1}^N \frac{N_{\text{win},i}}{\sigma_{\text{ns},i}^2} (\theta_i - \hat{\theta}_i)^2. \quad (10)$$

The loss terms for detection L_{detect} and communication L_{comm} are equal to (9).

C. Neural Network Training

The complete trained system is obtained in three phases: Pre-training, fine-tuning, and limiting. In pre-training, we first set $L_{\text{detect}} = 0$ and in a secondary pre-training step $L_{\text{angle}} = 0$ to initialize both sensing functionalities separately. We employ pre-training to establish the general behavior of the network. We use a total of $2.5 \cdot 10^7$ communication symbols for both pre-training steps, divided into mini-batches of 10^4 symbols. We use the Adam optimizer with a learning rate of 10^{-4} . The length of the sensing window is randomly chosen between 1 and 15 for each sensing state, to optimize for different N_{win} and give insight into the multi-snapshot behavior. Fine-tuning establishes the operating point of the JCAS trade-off. Fine-tuning is performed on $5 \cdot 10^7$ symbols by using the whole loss function in (8) starting with the parameters established in the pre-training. We use the same hyperparameters as used for pre-training. Lastly, limiting ensures that the constant false alarm rate is kept. In the

limiting phase, the system runs separately for 10^4 symbols for each length of the sensing window N_{win} . The neural network components are not trained anymore in this phase, but the decision threshold for detection is refined as described in [8].

For validation of the communication component, we choose the BER as a metric. The object detection task is evaluated on the basis of its detection rate and false alarm rate. For easier comparison, we design detectors with a constant false alarm rate. The AoA estimation is evaluated on the root mean squared error (RMSE) of angle estimates of all targets.

IV. SIMULATION RESULTS AND DISCUSSION

In our simulations, the communication receiver is located at an AoA of $\varphi \in [30^\circ, 50^\circ]$. Radar targets are found in a range $\theta \in [-20^\circ, 20^\circ]$. Our monostatic transmitter and sensing receiver are both simulated as a linear array with $K = 16$ antennas and we consider an observation window up to $N_{\text{max}} = 15$ and use a 16QAM as modulation format. For the radar receiver, our objective is to achieve a false alarm rate of $P_f = 10^{-2}$ while optimizing the detection rate and angle estimator.

A. Benchmarks for Modulation, Detection and Angle Estimation

As a benchmark detector, we employ a generalized power detector based on a Neyman-Pearson detector [11, Chap. 10], distinguishing between two normal distributions of mean 0 with different variances. In the reference detector, the average power of all the input samples $z_{s;i,l}$ considered for sensing is computed. The detector can be formulated as

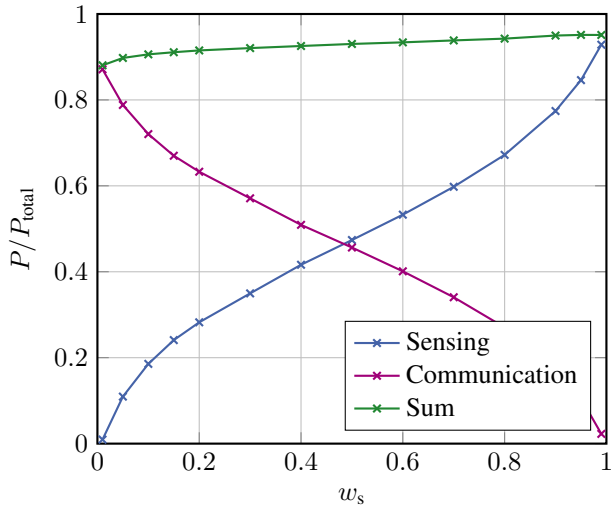
$$\frac{2}{\sigma_{\text{ns}}^2} \sum_{l=1}^{N_{\text{win}}} \sum_{i=1}^K |z_{s;i,l}|^2 \underset{\hat{t}=0}{\overset{\hat{t}=1}{\gtrless}} \chi_{2KN_{\text{win}}}^2 (1 - P_f), \quad (11)$$

with the chi-squared distribution $\chi^2(\cdot)$ with parameter $2KN_{\text{win}}$ denoting the degrees of freedom of the distribution. The correction factor is caused by the transformation of the problem from complex to real numbers, therefore artificially doubling the number of samples but reducing the noise by a factor of $1/\sqrt{2}$. The benchmark detector has a constant false alarm rate along varying values of SNR_s and N_{win} .

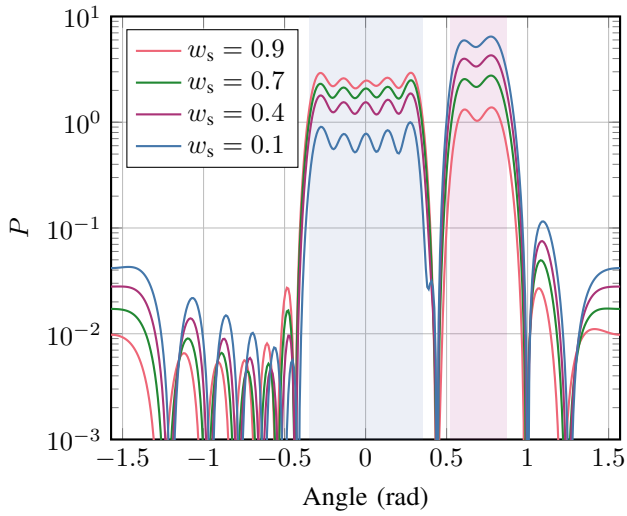
We use the well-studied ESPRIT algorithm as a benchmark for angle estimation as presented in [11]. ESPRIT performs close to the CRB for high SNRs or increasing observation windows N_{win} .

B. Beamforming Results

Figure 2(a) shows the effect of the trade-off parameter w_s on the power radiated to our areas of interest. We observe a linear relationship between w_s and the power $P = \int_{\theta=\theta_{\text{min}}}^{\theta_{\text{max}}} \beta(\theta)\sigma_s^2 d\theta$ in the region $[\theta_{\text{min}}, \theta_{\text{max}}]$, which is closely related to our beamforming gain β . When $w_s = 0.5$, the power is almost evenly distributed between sensing and communication. However, for $w_s < 0.2$ and $w_s > 0.8$, the trade-off becomes less linear, with the radiated power geared toward the less favored function decreasing more quickly. The total power radiated in both areas of interest increases



(a) Power distribution for communication receiver at $30 \dots 50^\circ$ and sensing object at $-20 \dots 20^\circ$



(b) Beam patterns outputs

Fig. 2. Beamforming results for varying SNR_c at different operating points w_s . The sensing area is filled light blue, the communication area light purple.

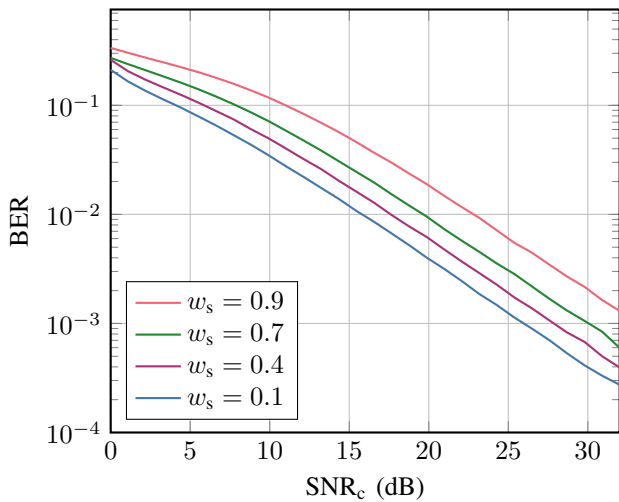


Fig. 3. Communication results for varying SNR

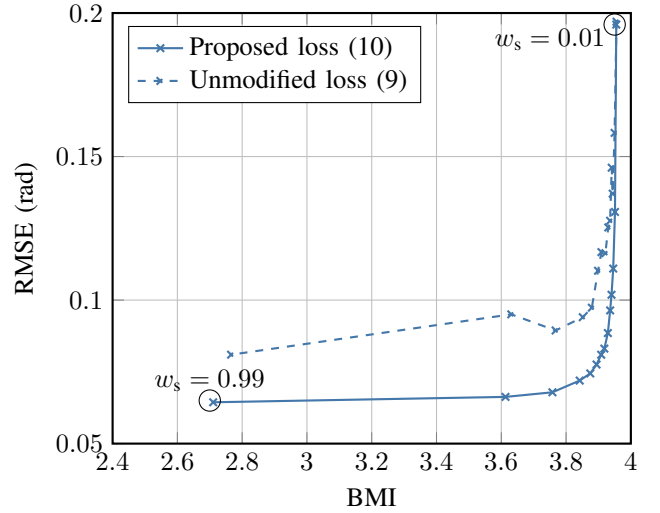


Fig. 4. QAM operating at different w_s after training with the modified loss function and without (dashed). Performance evaluated at $\text{SNR}_c = 20.8$ dB, $\text{SNR}_s = 2.6$ dB and $N_{\text{win}} = 1$

slightly with increasing w_s , while around 10% of the power is consistently radiated outside of our areas of interest. In Fig. 2(b), the beam patterns for certain values of w_s are displayed. The area for sensing is marked in light blue, while the area for communications is marked in light purple. We can see that most of the energy is radiated in our areas of interest and how the power is traded off between the two regions. We observe that more power is radiated outside our area of interest when only communication is performed, which is due to higher side lobes, particularly at an angle of $\pm 90^\circ$.

C. Communication Results

Previous works [4], [5] have demonstrated that NNs can be trained effectively as demappers. Figure 3 displays the BER for a range of SNR values and different trade-off factors w_s . As expected, we observe a higher BER as function of the raw SNR_c when increasing w_s . This degradation can be attributed to the beamforming gain towards the communication receiver, as the modulation format is identical for all w_s .

D. Angle Estimation Results

We analyze the effect of the modified angle loss term on the results compared to the unmodified loss given in (9) in Fig. 4. We observe possible operating points of the JCAS system that can be attained by selecting a different trade-off factor w_s . With the original loss function (9), as indicated by the dashed lines, the trained angle estimator demonstrates unsatisfactory performance. During training, we also noticed unreliable convergence of the system. We would anticipate a monotonic behavior of the curves, from high w_s in the left bottom corner of the plot to low w_s in the upper right corner. Without the modified loss function, there are performance fluctuations. The loss function is needed to optimize the neural network based on gradients with respect to the NN weights. However, after training with the unmodified loss, the estimation error depends mainly on the noise power and N_{win} . Since N_{win} and

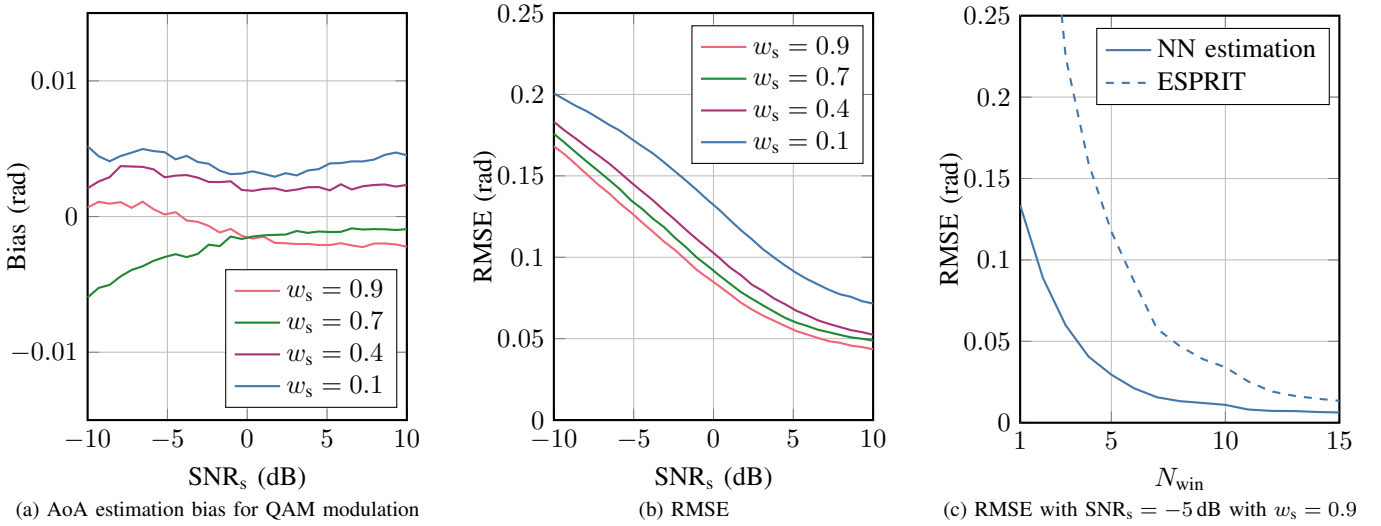


Fig. 5. AoA estimation results evaluated on different SNR for single snapshot sensing

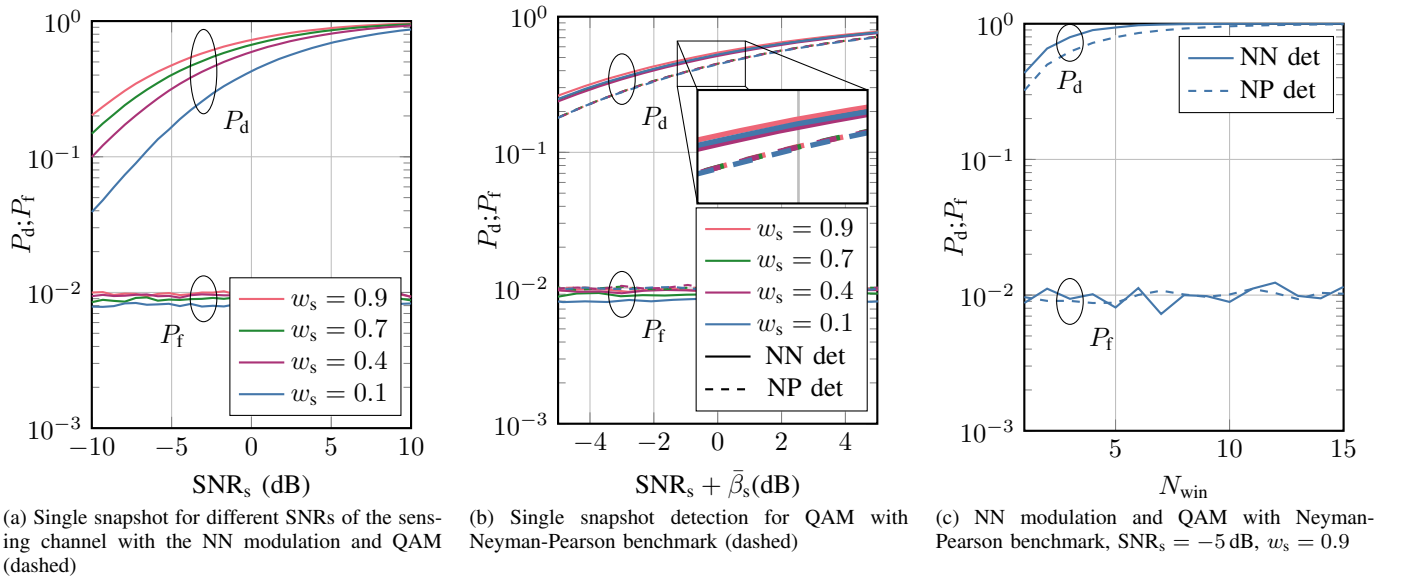


Fig. 6. Detection probability and false alarm rate for varying SNR

σ_{ns} are randomly chosen from uniform distributions during training, the loss is influenced by random processes which distort the magnitude of the gradients. Nevertheless, this randomness during training is beneficial for generalization. By modifying the loss function, we keep the randomness in our training data while normalizing the expected magnitude of the gradients. We achieve the gradual performance trade-off as expected and achieve a lower RMSE of the AoA estimation than for the unmodified loss while a similar BMI is achieved.

Results with a single target were already presented in [2], [8]. In Fig. 5(a), we analyze the estimation bias of the trained AoA estimator. Since we use the formulation of the CRB for an unbiased estimator, we should check for large biases that might cause unwanted effects in our system. The trained estimators lead to small biases in the order of 10^{-2} . We do not observe a clear trend of the bias as a function of SNR or w_s , nor do we observe a systematic bias. In Fig. 5(b), we can observe how increasing w_s decreases the

angle estimation error for single snapshot sensing, as well as how the RMSE decreases with increasing SNR. The slope of the RMSE flattens for higher SNR. In Fig. 5(c), we compare the RMSE of AoA estimation for different window lengths N_{win} . The trained angle estimators outperform ESPRIT at a raw $\text{SNR}_s = -5$ dB. At low SNR, the proposed method can consistently outperform the ESPRIT baseline.

E. Detection Results

In Fig. 6(a), we evaluate target detection with varying SNR. The false alarm rate is kept approximately constant at $P_f \approx 10^{-2}$, as intended by design. Since we numerically calculate an appropriate decision threshold T_{off} for each system, we observe small variations. The detection probability P_d increases with w_s , indicating the impact of beamforming, especially for very low w_s , where the beamformer barely illuminates the sensing area. A detection rate of 0.5 is obtained only at $\text{SNR}_s = 2$ dB for $w_s = 0.1$.

In Fig. 6(b), we show the trained detectors together with the baseline detector but correct the SNR with the average beamforming gain $\bar{\beta}_s$. We can observe that the benchmark detector leads to a lower detection rate, as it cannot take directional information into account. All detectors trained for QAM perform almost identically.

In Fig. 6(c), we evaluate the detection performance for different observation window lengths N_{win} . Increasing N_{win} improves the detection rate. The false alarm rate remains approximately at P_f for varying N_{win} for all trained detectors, although it tends to vary more than for different SNRs. As we normalize the signal at the sensing receiver to the same noise floor, while numerically calculating separate thresholds for each N_{win} , this is expected.

V. CONCLUSION

In this paper, we have proposed a novel loss function for JCAS systems based on supervised learning. By separating the loss function from the SNR and observation window length for sensing, we have achieved a more reliable convergence of our system and improved its overall performance. We were able to adjust the trade-off between sensing and communication performance using the trade-off factor w_s . The trained object detector and AoA estimator both outperform the baseline algorithms, namely a Neyman-Pearson-based power detector for object detection and ESPRIT for AoA estimation. Having reviewed the effects of multi-snapshot estimation encourages us not to use each communication sample to perform sensing by itself in scenarios where objects are

slow enough to be captured by multiple samples in almost the same position.

REFERENCES

- [1] T. Wild, V. Braun, and H. Viswanathan, "Joint design of communication and sensing for beyond 5G and 6G systems," *IEEE Access*, vol. 9, 2021.
- [2] J. M. Mateos-Ramos, J. Song, Y. Wu, C. Häger, M. F. Keskin, V. Yajnanarayana, and H. Wymeersch, "End-to-end learning for integrated sensing and communication," in *Proc. IEEE Int. Conf. Commun. (ICC)*, 2022.
- [3] J. M. Mateos-Ramos, C. Häger, M. F. Keskin, L. L. Magoarou, and H. Wymeersch, "Model-based end-to-end learning for multi-target integrated sensing and communication," 2023, arXiv 2307.04111, submitted to JSTSP.
- [4] T. O'Shea and J. Hoydis, "An introduction to deep learning for the physical layer," *IEEE Trans. Cogn. Commun. Netw.*, vol. 3, no. 4, 2017.
- [5] S. Cammerer, F. Ait Aoudia, S. Dörner, M. Stark, J. Hoydis, and S. ten Brink, "Trainable communication systems: concepts and prototype," *IEEE Trans. Commun.*, vol. 68, no. 9, pp. 5489–5503, 2020.
- [6] M. P. Jarabo-Amores, R. Gil-Pita, M. Rosa-Zurera, F. López-Ferreras, and R. Vicen-Bueno, "MLP-based radar detectors for Swerling 1 targets," *Proc. Pattern Recognit. Image Analysis*, vol. 18, no. 1, pp. 101–106, 2008.
- [7] J. Fuchs, A. Dubey, M. Lubke, R. Weigel, and F. Lurz, "Automotive radar interference mitigation using a convolutional autoencoder," in *Proc. IEEE Int. Radar Conf. (RADAR)*, 2020.
- [8] C. Muth and L. Schmalen, "Autoencoder-based joint communication and sensing of multiple targets," in *Proc. WSA/SCC*, Jan. 2023.
- [9] C. Sturm and W. Wiesbeck, "Waveform design and signal processing aspects for fusion of wireless communications and radar sensing," *Proc. IEEE*, vol. 99, no. 7, 2011.
- [10] M. Braun, C. Sturm, and F. K. Jondral, "Maximum likelihood speed and distance estimation for OFDM radar," in *Proc. IEEE Radar Conf.*, 2010.
- [11] H. L. van Trees, *Optimum Array Processing: Part IV of Detection, Estimation, and Modulation Theory*. Wiley, 2002.